ACS Catalysis

Research Article

pubs.acs.org/acscatalysis

Following the Creation of Active Gold Nanocatalysts from Phosphine-Stabilized Molecular Clusters

John Kilmartin,[†] Rozie Sarip,[†] Ricardo Grau-Crespo,[†] Devis Di Tommaso,[†] Graeme Hogarth,[†] Carmelo Prestipino,[‡] and Gopinathan Sankar*[,†]

[†]Department of Chemistry, University College London, 20 Gordon Street, London WC1H 0AJ, U.K.

[‡]Sciences Chimiques de Rennes UMR 6226, Matériaux Inorganiques, Chimie Douce et Réactivité (MICDR), Campus de Beaulieu, Bât 10B F-35042 Rennes, France

Supporting Information

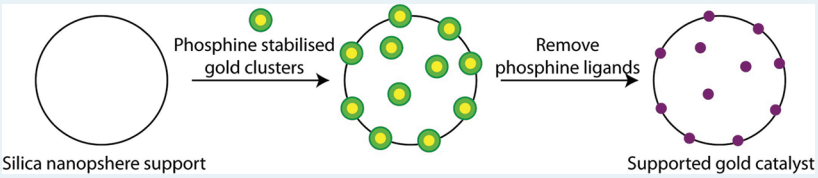

ABSTRACT: The phosphine-stabilized gold cluster $[Au_6(Ph_2P\text{-}o\text{-tolyl})_6](NO_3)_2$ is converted into an active nanocatalyst for the oxidation of benzyl alcohol through low-temperature peroxide-assisted removal of the phosphines, avoiding the high-temperature calcination process. The process was monitored using in situ X-ray absorption spectroscopy, which revealed that after a certain period of the reaction with tertiary butyl hydrogen peroxide, the phosphine ligands are removed to form nanoparticles of gold which matches with the induction period seen in the catalytic reaction. Density functional theory calculations show that the energies required to remove the ligands from the $[Au_6L_n]^{2+}$ increase significantly with successive removal steps, suggesting that the process does not occur at once but sequentially. The calculations also reveal that ligand removal is accompanied by dramatic rearrangements in the topology of the cluster core.

KEYWORDS: *gold catalysts, molecular clusters, oxidation, X-ray absorption spectroscopy, EXAFS, XANES, density functional theory*

INTRODUCTION

Oxidation reactions are of enormous industrial importance, especially in the synthesis of fine chemicals. Stoichiometric quantities of oxidizing agents such as permanganate are widely utilized in industrial oxidation reactions which lead to the accumulation of byproduct. A green alternative would be a reusable (heterogeneous) catalyst that could oxidize the desired substrate without forming side products. It has been shown that using an oxygen source such as hydrogen peroxide, molecular oxygen or nitrous oxide, a clean industrial oxidation processes may be established.[1−8]

Gold is now recognized as being unique among the metals for its catalytic oxidation activity, specifically for the oxidation of CO to CO_2 at low temperatures.[9,10] It has been established that there is a strong dependency of the activity of the gold catalyst on the size of the gold particles present.[9−13] Recently, it was implicated that the active component of the catalyst for this reaction was not the large nanoparticles (>1 nm) of gold, but the small clusters of gold atoms only ∼0.5 nm or less in size.[14,15] Previously reported studies hinted at this when molecular clusters deposited on titania yielded highly active catalysts for oxidation of CO[16] and in addition to this several organic substrates have been converted to their respective oxidized products using supported gold catalysts.[3,17−21] One reaction of particular interest is the oxidation of benzyl alcohol to benzaldehyde.[22−27]

A major limitation in the synthesis of supported gold nanoparticle catalysts is the lack of control over the size of the particles formed. One approach to address this issue is to use molecular clusters as catalyst precursors; such an approach has been successfully used, for example, to produce a variety of mono and bimetallic clusters.[28−30] In particular, studies by Iwasawa and co-workers have focused on the use of gold-phosphine precursors to generate supported gold nano particles.[16,31] In this communication we report the successful preparation of catalytically active gold nanoparticles using a phosphine-stabilized molecular gold clusters as a precursor.

It is well-known that both the size and shape of phosphine-stabilized molecular gold clusters can be easily tuned as a function of the size and donor properties of the phosphine ligands. For our initial studies we identified the hexanuclear gold cluster $[Au_6(Ph_2P\text{-o-tolyl})_6](NO_3)_2$ (Figure 1) as a precursor since it is easily synthesized in high yields. We supported the generated nanoparticles on silica nanospheres of *ca.* 500 nm in diameter (for ease of characterization since they have a more regular surface than that of fumed silica).

Although thermal methods are traditionally used for the removal of phosphine ligands to generate naked gold

Received: November 30, 2011
Revised: April 16, 2012
Published: April 18, 2012

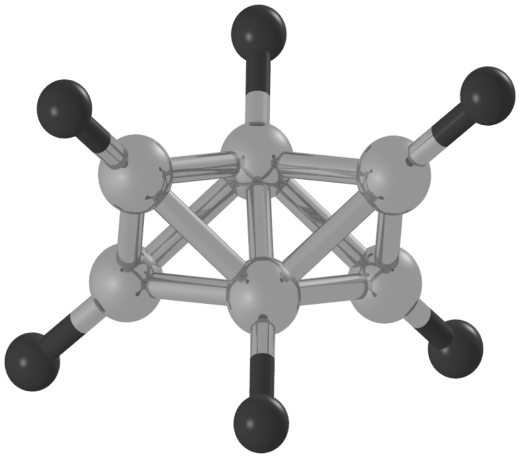

Figure 1. Cluster core geometry of $[Au_6(Ph_2P\text{-}o\text{-}tolyl)_6]^{2+}$. Carbon and hydrogen atoms have been omitted for clarity. Dark and light colored circles represent phosphorus and gold atoms, respectively.

nanoparticles,[32−34] we found that these nanoparticles can also be generated by a soft chemical process using organic hydrogen peroxide at temperatures below 100 °C. We have followed the reaction of converting phosphine-stabilized gold clusters to nanoparticles in a liquid−solid mixture using in situ X-ray absorption spectroscopy, at the Au L_{III} edge, a technique that is sensitive to local coordination changes.[11,12,35−38] The results suggest that *tert*-butyl hydrogen peroxide (TBHP), which is used as the oxidant for the catalytic reaction, assisted the removal of the phosphine ligands to generate the active gold catalysts.

EXPERIMENTAL SECTION

$[Au_6(Ph_2P(o\text{-}tolyl)_6)](NO_3)_2$ Synthesis. $[Au_6(Ph_2P(o\text{-}tolyl)_6)](NO_3)_2$ was synthesized using the method described by Briant and co-workers.[39,40]

Catalyst Preparation. Clusters were deposited onto the silica or alumina support by dissolving the $[Au_6(Ph_2P\text{-}o\text{-}tolyl)_6](NO_3)_2$ clusters (0.1 g, 0.03 mmol) in (∼5 mL) methanol and adding this to a suspension of the support (1 g of silica nanospheres with 500 nm diameter) to yield ∼4 wt % of gold supported on silica. The container was sealed and placed in an ultrasonic bath for 5 min to obtain a good dispersion of the support. The mixture was then stirred for 1 h and after this time was placed in an ultrasonic bath for another 5 min. The solvent was then removed under vacuum leaving a coating of the clusters on the surface of the alumina or silica nanospheres. The actual gold loading, estimated based on atomic absorption spectroscopy, is found to be 1.808×10^{-4} mmol for the uncalcined catalysts and 1.726×10^{-4} mmol for the calcined catalyst.

Catalysis Experiments. In a typical reaction, 0.20 g of catalyst was weighed in to a reactor vessel. To this, 5.4 mL (26.06 mmol) of benzyl alcohol (Sigma Aldrich) and 5.67 mL (5.0−6.0 M in decane) of *tert*-butyl hydroperoxide was added. After placing the reactor in to the temperature controller, it was fitted with a condenser and heated to 95 °C, while being stirred. Samples of the reaction mixture were collected at time zero and then every 15 min of the first hour and every hour from then until 4 h when the reaction was stopped by cooling the mixture to 5 °C. The samples were analyzed using a PerkinElmer Clarus 500 Gas Chromatograph.

QEXAFS. X-ray absorption spectroscopic study, at the Au L_{III} edge, was carried out at BM29[41] of ESRF (which operates at 6GeV). In a typical experiment, 150 mg of self-supporting wafer of supported gold cluster catalysts was placed into the in situ cell, TBHP was added and the cell was sealed prior to placing the cell in a heating block (Kapton films were used as window material). The cell is made of brass with a PEEK insert having a hole of ∼15 mm diameter, which contains the liquid/solid sample (a picture of the in situ cell is given in the Supporting Information). A separate block containing cartridge heaters was used as the heating block into which the cell can be inserted and heated to a specific temperature of up to 200 °C. In this experiment the cell was heated to 95 °C at the rate of 6 °C/min and the data collection was started when the temperature of the cell was 30 °C. Au L_{III} XAS data were collected over the energy range of 11.6−13.0 keV, using transmission geometry. The whole scan was performed over 8 s and an additional 8 s was required to move the monochromator back to the starting position. A double crystal Si(111) monochromator was used for this work and ion chambers were employed to record incident (I_o) and transmitted beam intensities; measurements were performed using transmission geometry. Ten scans were averaged to obtain a better quality data. Only selected data sets were analyzed, since we did not see much change in the beginning and at the onset of the reaction (removal of ligand), every data set (averaged over 10 scans) were analyzed. The data collected was processed using VIPER[42] and EXCURVE software.[43] Au−P and Au−Au phase shifts and amplitude factors were calculated within the EXCURVE software. Au foil was used as the reference to estimate the amplitude reduction factor and this was kept constant for the analysis of Au clusters. We analyzed only the first and second neighbors, Au−P and Au−Au coordination spheres within 3 Å, hence multiple-scattering methodology was not employed in this analysis. The raw data were processed without Fourier filtering and the analysis was performed in *k*-space. Electron microscope images were collected on a 100 keV Transmission electron microscope and a JEOL JSM-6301F Field Emission scanning electron microscope.

DFT Calculations. Density functional theory calculations were performed with a Perdew−Burke−Ernzerhof (PBE) exchange-correlation functional[44] using the DMol3 code.[45] In DMol3, the electronic wave function is expanded in a basis set of localized atom-centered functions, which are defined numerically on a dense radial grid. For geometry optimizations we employed a double numerical basis set (DND) with a polarization d-function on all non-hydrogen atoms, with each basis function restricted to within a cutoff radius of R_{cut} = 4.0 Å. More accurate total energies were then computed for the optimized geometries, by including a polarization p-function on all hydrogen atoms (DNP), and setting the cutoff radius for each basis function to 4.7 Å. The inner core−electrons for Au were represented by semicore pseudopotentials, which were generated by fitting to all-electron relativistic DFT results, and specifically developed to improve the accuracy of DMol3 calculations.

RESULTS AND DISCUSSION

First, we discuss some of the catalytic results and subsequently show the correlation between these and the in situ X-ray absorption spectroscopic studies.

In a typical ex situ study of the catalytic reaction, the catalysts were calcined at 300 °C, in order to remove the stabilizing

dx.doi.org/10.1021/cs2006263 | ACS Catal. 2012, 2, 957−963

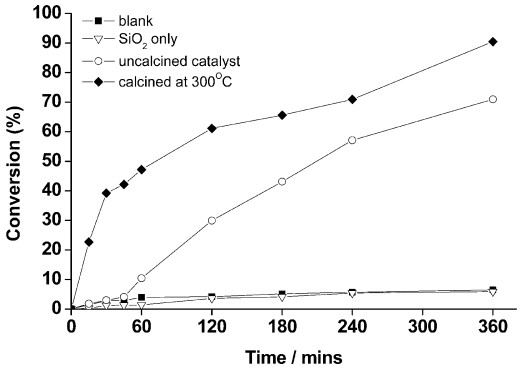

Figure 2. Graph comparing the catalytic activities of supported clusters calcined at 300 °C and uncalcined. The uncalcined catalyst shows very low initial conversion whereas the calcined catalyst gives high activity from the onset of the reaction.

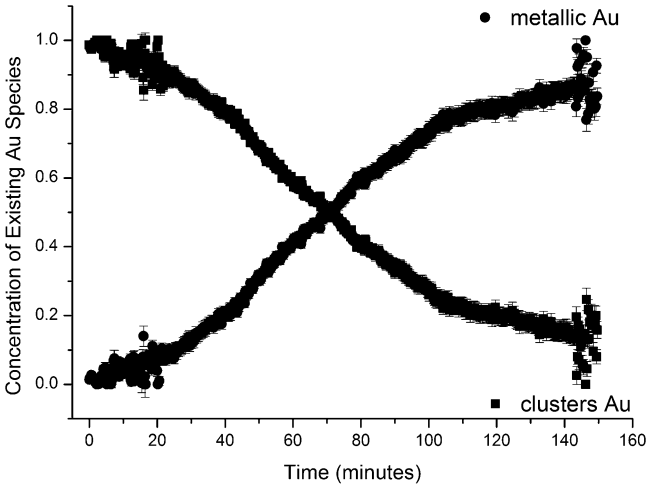

Figure 4. Plot of the change in fractions of cluster Au and metallic Au obtained from the linear combination fitting analysis using Athena software.

phosphine ligands and to generate supported gold nanoparticles. These proved to be active for benzyl alcohol oxidation, particularly when used in conjunction with *tert*-butyl hydroperoxide (TBHP in decane) as an oxygen source. In particular, the calcined catalyst shows conversion without any induction time and the final conversion of benzyl alcohol, after 3 h of reaction, is estimated to be 90% (Figure 2) (with up to 90% selectivity for benzaldehyde) without the need for high pressure conditions; other expected products are benzoic acid and benzyl benzoate. We estimated the initial rate for benzaldehyde conversion (by taking into account the Au loading to obtain the change of turn over number (TON) per unit of time, calculated between 15 and 60 min) to be = 1645 min^{-1}. However, during the process of removing the phosphine ligands through calcination, the naked clusters were found to be highly mobile on the support surface leading to significant aggregation and thus the formation of relatively large gold particles (20−70 nm; see Supporting Information for TEM images and XRD diffractograms).

During the course of a systematic study to investigate the effect of calcination temperature, we carried out the same catalytic reaction using uncalcined catalysts (as supported) which contained the phosphine ligands. Interestingly, it was found that the uncalcined clusters were also active for benzyl alcohol oxidation, in presence of TBHP, although initially to a lesser extent than the calcined gold catalysts. When carrying out the catalytic reactions, it was noted that there was an induction

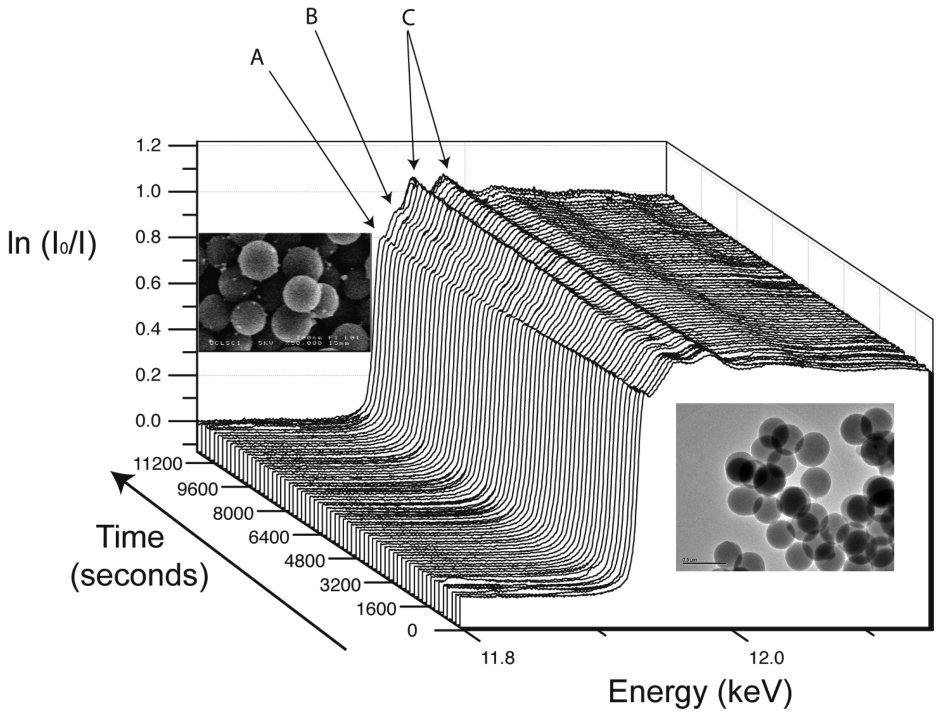

Figure 3. Au L_{III} edge XANES data highlighting the gradual loss of feature **A**, the development of feature **B** and the accentuation of features **C**. Feature **A** is lost as the reaction proceeds due to loss of phosphine ligands and formation of metallic particles. Typical TEM images of the as synthesized catalyst (bottom right) and denuded catalyst (top left) are also shown here, which highlights the absence of any gold cluster in the as prepared state and formation of nano particles after reaction.

dx.doi.org/10.1021/cs2006263 | *ACS Catal.* 2012, 2, 957−963

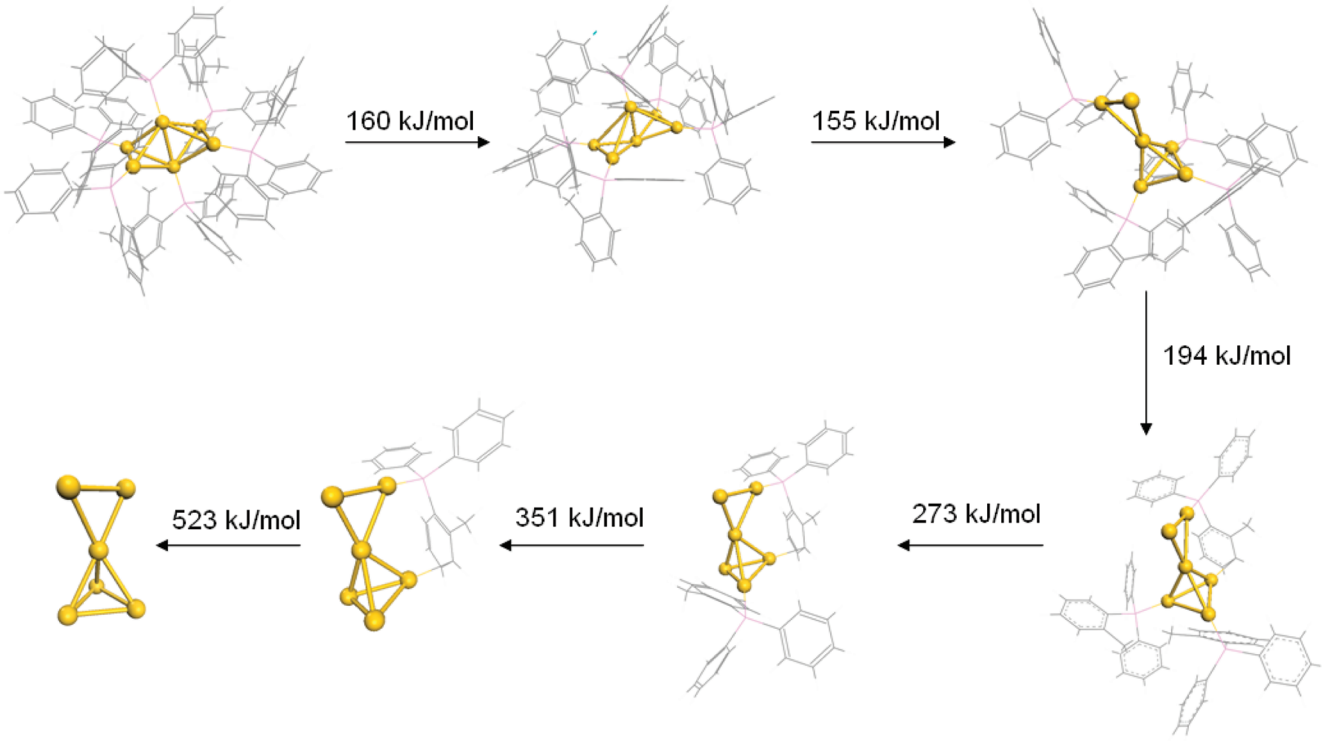

Figure 5. Minimum energy path for ligand removal in the $[Au_6L_n]^{2+}$ cluster and the energies required for each step, according to density functional theory calculations.

period of ~30 min, before the catalyst showed activity. Thus for the first 30 min, little to no conversion of the benzyl alcohol was observed. In Figure 2, we compare the conversion (benzyl alcohol) versus time for the catalysts calcined in air at 300 °C and the uncalcined catalysts; we have also given results for the blank reactions performed with pure silica support and without any solid to show the effect of catalysts in the reaction. The initial rate of reaction was estimated (similar to the calcined catalysts, but between 45 and 90 min, since there was an induction period of *ca.* 30 min) to be 1032 min^{-1}, which appears to be less than that of the calcined catalyst, despite the smaller particle size of the uncalcined catalyst. This may be due to the consumption of part of the hydrogen peroxide for removal of the phosphine ligands which would affect the concentration of available peroxide for the catalytic reaction and therefore the reaction rate. The lack of activity during the induction period seen for the uncalcined catalysts is thought to be due to the protective nature of the phosphine ligands which shroud the active sites and once the denuded clusters are exposed to the reactants (by removing the phosphine ligands), the conversion begins; over six hours, the uncalcined catalyst achieves a conversion of ~70%. Note that the conversion is not as high as that of the calcined catalyst, since some of the peroxide is used for the removal of phosphine ligands as phosphine oxide.

To establish that phosphine removal takes place prior to the catalysis, we used a specially designed in situ reactor cell to carry out in situ X-ray absorption spectroscopy (at the Au L_{III} edge) at 95 °C. Using this procedure we were able to design an experiment that allowed us to observe the reaction of gold cluster compound with TBHP at similar temperatures to those in the catalytic (batch) reactor (we did not add benzyl alcohol in this reaction mixture, since excess amount of liquid absorbs more X-rays, which affected the quality of data; furthermore, it is unlikely that benzyl alcohol alone would have assisted the removal of the ligands). Rapid in situ EXAFS were employed to monitor the gold in real time as the reaction proceeded. Stacked Au L_{III} XANES data (normalized) recorded in situ is shown in Figure 3. Comparison with the data reported in literature[46,47] clearly indicates that the features marked **A** and **C** (Figure 3) at the start of the reaction resemble those of materials containing gold surrounded by phosphine ligands. During the course of the reaction these features undergo considerable changes; in particular, the appearance of a shoulder **B**, while feature **A** decreases in intensity and **C** becomes well-defined. The final spectrum resembles that of metallic gold. In order to obtain a more quantitative picture of the changes taking place during the reaction, we analyzed the XANES data using linear combination fit analysis method, taking the XANES data of the starting material and metallic gold as reference. Fractions of the starting cluster compound and metallic gold present in the system with time are plotted in Figure 4. No appreciable change was seen for the first 20 min and after this time, the features due to cluster begin to decrease with concomitant increase in the metallic component. These changes take place gradually over ~100 min and there was no abrupt conversion of the cluster to metallic gold. Appreciable change in the catalytic conversion was seen only above 40 min. This could be due to the initial loss of some phosphine ligands (as oxide) allowing rearrangement of the cluster. Removal of phosphine ligands from the cluster leaves a formal positive charge (0.33|e| per Au) delocalized over the gold atoms. Our experiments indicate that the final state of gold is metallic, that is in a fully reduced state; microscopic data also supports the presence of metallic particles. It is possible to speculate that the reduction of gold is related to the presence of noninnocent anions in solution (nitrate in our case) which might provide electrons to the clusters. It is likely that such a reduction would

dx.doi.org/10.1021/cs2006263 | *ACS Catal.* 2012, 2, 957–963

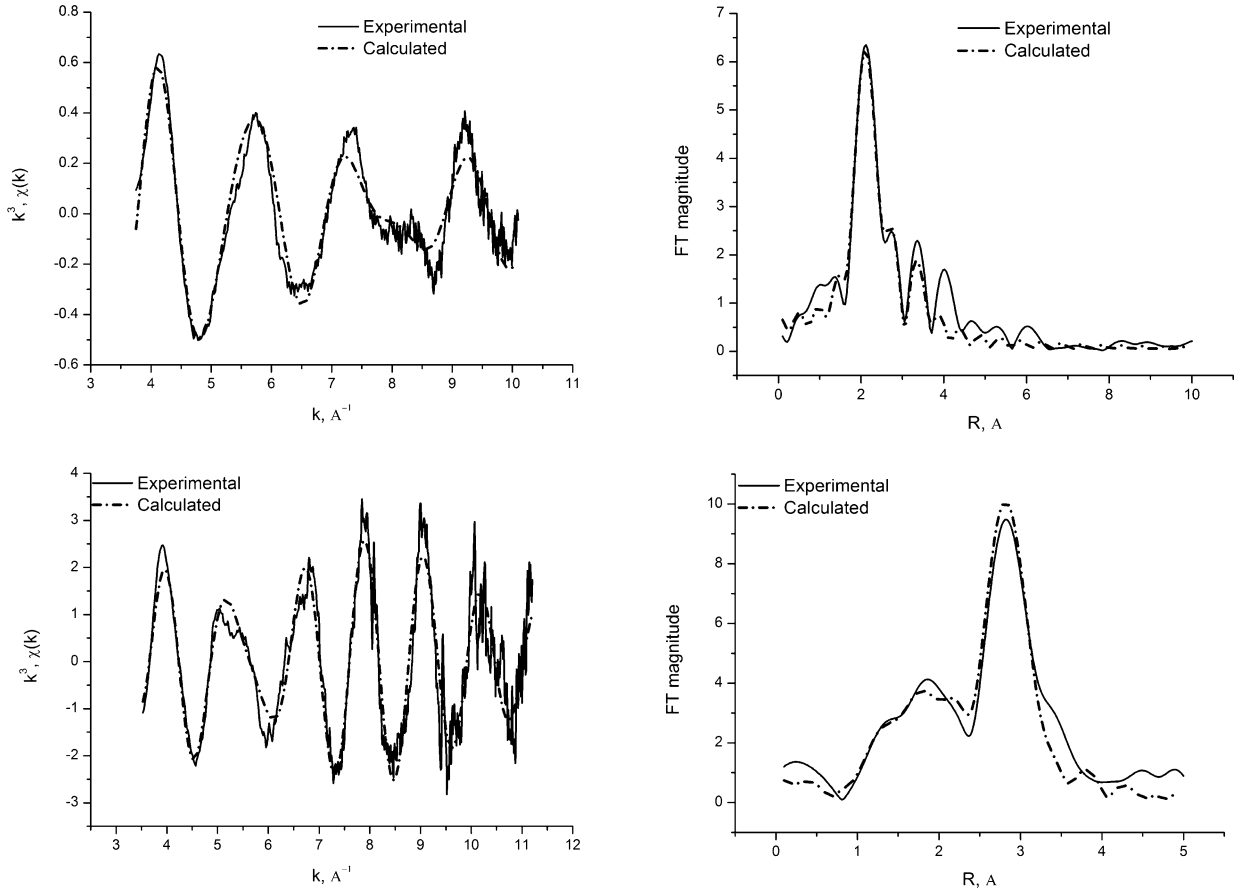

Figure 6. Best fit between experimental Au L_{III} edge EXAFS and calculated data for Au clusters catalyst at the beginning of in situ EXAFS experiment (top) and at after 150 min (bottom). On the right the corresponding Fourier transforms of the experimental and calculated data are shown. Note that the EXAFS data of 15 scans (recorded over 3 min) are combined to obtain a good signal-to-noise.

Table 1. Structural Parameters Derived from the Analysis of Au L_{III} EXAFS of the Starting Supported Au_6 Cluster on Silica and after Reaction Over 150 Minutes with TBHP

reaction time (min)	atom pair	N	R (Å)	σ^2 (Å^2)	fit index
0	Au−P	1.5	2.25	0.006	41.29
	Au−Au	3.45	2.74	0.012	
150	Au−P	0.3	2.28	0.01	35.64
	Au−Au	8.7	2.84	0.012	

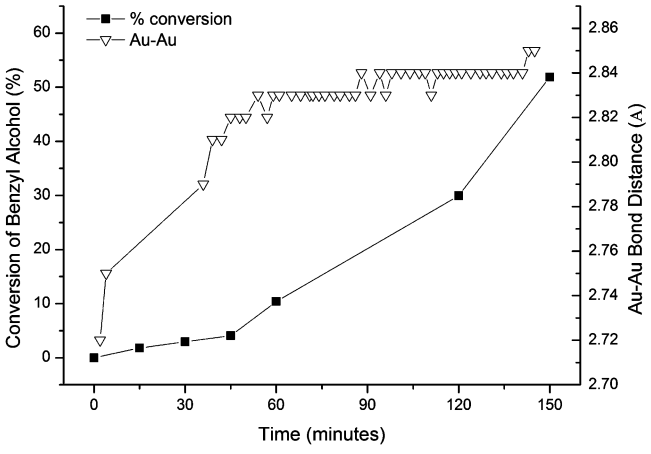

Figure 7. Catalytic performance of the uncalcined Au catalyst and the changes of Au−Au bond distances over time.

occur via interaction of these anions with the totally or partially naked positive gold clusters (that is, after the removal of some or all of the ligands), but clearly further work is necessary to verify these routes.

Quantum mechanical calculations provide useful insight into the energetics and dynamics of the ligand removal process. Starting from $[Au_6(Ph_2P(o\text{-tolyl})_6)]^{2+}$, we calculated the energies for the removal of ligands from the cluster, following the sequence:

$$[Au_6L_6]^{2+} \rightarrow [Au_6L_5]^{2+} \rightarrow [Au_6L_4]^{2+} \rightarrow [Au_6L_3]^{2+} \rightarrow [Au_6L_2]^{2+} \rightarrow [Au_6L]^{2+} \rightarrow [Au_6]^{2+}$$

where L = $Ph_2P(o\text{-tolyl})$. For the sake of computational simplicity, and based on the arguments given above, we have assumed here that the ligand removal process precedes the reduction of the clusters, and therefore the positive charge is conserved until the last stage of ligand removal. At each step, the energy was calculated with respect to an isolated neutral phosphine molecule. Since the configurational space associated with this ligand removal process is too large for an exhaustive computational screening, we have considered only the minimum-energy pathway, which results from the following procedure: at each step n we generate configurations by taking away one ligand from the most stable configuration obtained in step $n - 1$. This corresponds to the most likely path for ligand removal and should be illustrative of the process, although of course many other paths will also occur in practice. Figure 5

dx.doi.org/10.1021/cs2006263 | ACS Catal. 2012, 2, 957−963

shows the structures and the energies found for each step. The removal of the first two ligands involves much lower energies than that of subsequent ligands, for which increasing energies are required. Since the activation barriers for ligand removal have to be higher than the removal energies, this result suggests that the phosphine ligands are not lost simultaneously but gradually. It is also interesting to observe that the removal of phosphine ligand leads to significant rearrangements of the cluster, changing the topology of the Au_6 cluster core.

Analysis of the EXAFS data appears to be more complex, in particular after 10 min of the reaction, since the Au−Au coordination associated with the cluster and formed naked gold particles coexist resulting in large disorder around gold atoms. Hence, we analyzed the EXAFS data collected at the initial stages and final stages in detail. The results, in particular coordination number (due to high-correlation with disorder parameter−Debye−Waller factor) is found to be unreliable for the data collected between 15 and 75 min. The analysis of the Au L_{III} EXAFS data of the samples recorded during the initial stages of the reaction revealed the presence of Au−P (at 2.24 Å with a coordination number of 1.6) and Au−Au (at 2.74 Å with a coordination number of 3.5) coordination and best fit to the EXAFS data and the associated Fourier transform (FT) are shown in Figure 6. These numbers remained constant for first *ca.* 10 min and after this time, the Au−P coordination number decreased and Au−Au increased over a period of time. As mentioned earlier, coexistence of the two types of system did not allow us to obtain reliable structural information. This we believe could be due to the partial removal of phosphine ligands at this stage and possible reorganization of the cluster until a stable metal particle is achieved upon removal of all the ligands. The best fit between experimental EXAFS data and the associated FT's of the data collected after ∼150 min are shown in Figure 6. The analysis clearly shows that Au−Au coordination dominates with a very small contribution from Au−P remains at this stage; it is difficult to determine whether some unreacted clusters or some of the phosphine remain attached to the gold nanoparticles. The Au−Au coordination number of ∼8.7 (Au−P coordination is ∼0.35) suggests the presence of nanoparticles. The results from the analysis of EXAFS data are summarized in Table 1.

Once the majority of the phosphine ligands are removed, more stable naked gold clusters are formed. It appears that formation of naked gold particles is necessary to initiate the onset of catalytic activity (Figure 7).

In summary, time-resolved in situ XAS studies clearly show that the presence of peroxide assists the removal of phosphine ligands at temperatures of ∼90 °C to create the active nanosized gold catalysts for oxidation processes without the need for calcination at elevated temperatures. The study not only shows detailed structural changes to the cluster during the induction period, but also how the denuded gold clusters are formed during the catalytic reaction.

■ ASSOCIATED CONTENT

Supporting Information

This material is available free of charge via the Internet at http://pubs.acs.org.

■ AUTHOR INFORMATION

Corresponding Author

*E-mail: g.sankar@ucl.ac.uk.

Notes

The authors declare no competing financial interest.

■ ACKNOWLEDGMENTS

We thank EPSRC and Royal Society for funding and ESRF for the provision of beam time and other facilities. We also thank Dr Ruth Ballesteros for useful discussions.

■ REFERENCES

(1) Arends, I.; Sheldon, R. A. *Top. Catal.* **2002**, *19*, 133−141.
(2) Corma, A.; Garcia, H. *Chem. Soc. Rev.* **2008**, *37*, 2096−2126.
(3) Hutchings, G. J.; Scurrell, M. S. *Cattech* **2003**, *7*, 90−103.
(4) Panov, G. I.; Dubkov, K. A.; Starokon, E. V. *Catal. Today* **2006**, *117*, 148−155.
(5) Parmon, V. N.; Panov, G. I.; Uriarte, A.; Noskov, A. S. *Catal. Today* **2005**, *100*, 115−131.
(6) Shiju, N. R.; Fiddy, S.; Sonntag, O.; Stockenhuber, M.; Sankar, G. *Chem. Commun.* **2006**, 4955−4957.
(7) Thomas, J. M.; Raja, R.; Sankar, G.; Bell, R. G. *Acc. Chem. Res.* **2001**, *34*, 191−200.
(8) Thomas, J. M.; Sankar, G. *Acc. Chem. Res.* **2001**, *34*, 571−581.
(9) Haruta, M. *Gold Bull.* **2004**, *37*, 27−36.
(10) Haruta, M. *J. New Mater. Electrochem. Syst.* **2004**, *7*, 163−172.
(11) Calla, J. T.; Davis, R. J. *Catal. Lett.* **2005**, *99*, 21−26.
(12) Calla, J. T.; Davis, R. J. *J. Phys. Chem. B* **2005**, *109*, 2307−2314.
(13) Uzun, A.; Ortalan, V.; Hao, Y. L.; Browning, N. D.; Gates, B. C. *Acs Nano* **2009**, *3*, 3691−3695.
(14) Haruta, A. *Chem. Rec.* **2003**, *3*, 75−87.
(15) Herzing, A. A.; Kiely, C. J.; Carley, A. F.; Landon, P.; Hutchings, G. J. *Science* **2008**, *321*, 1331−1335.
(16) Kozlov, A. I.; Kozlova, A. P.; Liu, H. C.; Iwasawa, Y. *Appl. Catal., A* **1999**, *182*, 9−28.
(17) Carrettin, S.; McMorn, P.; Johnston, P.; Griffin, K.; Hutchings, G. J. *Chem. Commun.* **2002**, 696−697.
(18) Comotti, M.; Della Pina, C.; Matarrese, R.; Rossi, M. *Angew. Chem., Int. Ed.* **2004**, *43*, 5812−5815.
(19) Hughes, M. D.; Xu, Y. J.; Jenkins, P.; McMorn, P.; Landon, P.; Enache, D. I.; Carley, A. F.; Attard, G. A.; Hutchings, G. J.; King, F.; Stitt, E. H.; Johnston, P.; Griffin, K.; Kiely, C. J. *Nature* **2005**, *437*, 1132−1135.
(20) Zhao, R.; Ji, D.; Lv, G. M.; Qian, G.; Yan, L.; Wang, X. L.; Suo, J. S. *Chem. Commun.* **2004**, 904−905.
(21) Zheng, N. F.; Stucky, G. D. *Chem. Commun.* **2007**, 3862−3864.
(22) Aschwanden, L.; Mallat, T.; Grunwaldt, J. D.; Krumeich, F.; Baiker, A. *J. Mol. Catal A: Chem.* **2009**, *300*, 111−115.
(23) Choudhary, V. R.; Dhar, A.; Jana, P.; Jha, R.; Uphade, B. S. *Green Chem.* **2005**, *7*, 768−770.
(24) Choudhary, V. R.; Dumbre, D. K. *Top. Catal.* **2009**, *52*, 1677−1687.
(25) Dimitratos, N.; Lopez-Sanchez, J. A.; Morgan, D.; Carley, A.; Prati, L.; Hutchings, G. J. *Catal. Today* **2007**, *122*, 317−324.
(26) Enache, D. I.; Knight, D. W.; Hutchings, G. J. *Catal. Lett.* **2005**, *103*, 43−52.
(27) Haider, P.; Kimmerle, B.; Krumeich, F.; Kleist, W.; Grunwaldt, J. D.; Baiker, A. *Catal. Lett.* **2008**, *125*, 169−176.
(28) Gates, B. C. *Nat. Nanotechnol.* **2008**, *3*, 583−584.
(29) Kulkarni, A.; Lobo-Lapidus, R. J.; Gates, B. C. *Chem. Commun.* **2010**, *46*, 5997−6015.
(30) Thomas, J. M.; Johnson, B. F. G.; Raja, R.; Sankar, G.; Midgley, P. A. *Acc. Chem. Res.* **2003**, *36*, 20−30.
(31) Kozlov, A. I.; Kozlova, A. P.; Asakura, K.; Matsui, Y.; Kogure, T.; Shido, T.; Iwasawa, Y. *J. Catal.* **2000**, *196*, 56−65.
(32) Yuan, Y. Z.; Asakura, K.; Kozlova, A. P.; Wan, H. L.; Tsai, K. R.; Iwasawa, Y. *Catal. Today* **1998**, *44*, 333−342.
(33) Yuan, Y. Z.; Asakura, K.; Wan, H. L.; Tsai, K.; Iwasawa, Y. *Chem. Lett.* **1996**, 129−130.
(34) Yuan, Y. Z.; Asakura, K.; Wan, H. L.; Tsai, K.; Iwasawa, Y. *Bull. Chem. Soc. Jpn.* **1999**, *72*, 2643−2653.

(35) Grunwaldt, J. D.; Kiener, C.; Wogerbauer, C.; Baiker, A. *J. Catal.* **1999**, *181*, 223−232.
(36) Haider, P.; Grunwaldt, J. D.; Seidel, R.; Baiker, A. *J. Catal.* **2007**, *250*, 313−323.
(37) van Bokhoven, J. A.; Louis, C.; T Miller, J.; Tromp, M.; Safonova, O. V.; Glatzel, P. *Angew. Chem., Int. Ed.* **2006**, *45*, 4651−4654.
(38) van Bokhoven, J. A.; Miller, J. T. *X-Ray Absorption Fine Structure-XAFS13* **2007**, *882*, 582−584.
(39) Briant, C. E.; Hall, K. P.; Mingos, D. M. P.; Wheeler, A. C. *J. Chem. Soc., Dalton Trans.* **1986**, 687−692.
(40) Briant, C. E.; Theobald, B. R. C.; White, J. W.; Bell, L. K.; Mingos, D. M. P. *J. Chem. Soc., Chem. Commun.* **1981**, 201−202.
(41) Prestipino, C.; Mathon, O.; Hino, R.; Beteva, A.; Pascarelli, S. *J. Synchrotron Radiat.* **2010**, *18*, 176−182.
(42) Klementev, K. V. *J. Phys. D: Appl. Phys.* **2001**, *34*, 209−217.
(43) Binsted, N.; *CCLRC Daresbury Laboratory* 1998.
(44) Perdew, J. P.; Burke, K.; Ernzerhof, M. *Phys. Rev. Lett.* **1996**, *77*, 3865−3868.
(45) Delley, B. *J. Chem. Phys.* **2000**, *113*, 7756.
(46) Benfield, R.; Dore, J. C.; Grandjean, D.; Kroll, M. *J. Alloys Compd.* **2004**, *362*, 48−55.
(47) Benfield, R. E.; Grandjean, D.; Kroll, M.; Pugin, R.; Sawitowski, T.; Schmid, G. *J. Phys. Chem. B* **2001**, *105*, 1961−1970.